Geophys. J. Int. (2006) **164,** 490–500 doi: 10.1111/j.1365-246X.2006.02814.x

The effects of three-dimensional structure on two-dimensional images of crustal seismic sections and on the interpretation of shear zone morphology

R. W. Hobbs,[1] B. J. Drummond[2] and B. R. Goleby[2]

[1] *University of Durham, Department of Earth Sciences, South Road, Durham DH1 3LE, UK. E-mail: hobbs@durham.ac.uk*
[2] *Geoscience Australia, GPO Box* 378, *Canberra ACT* 2601, *Australia*

Accepted 2005 September 22. Received 2005 September 22; in original form 2003 July 10

SUMMARY

Crustal scale seismic images provide information on the geometry of subsurface structure. In this paper we examine shear zones as they provide geometrical constraints on the evolution of the crust and as they provide pathways for the migration of mineral-rich fluids from the lower crust. However, they typically appear in seismic images of the deep crust as laterally continuous bands of discontinuous reflections with individual reflections often having high amplitudes. Geological mapping of exposed shear zones show them to have a complex 3-D structure yet crustal-scale seismic reflection surveys use single or at the most only a few profiles, and therefore only create 2-D images of these structures. The processing and imaging of the multifold common midpoint (CMP) data assumes that the seismic energy comes entirely from within the plane of the section. In this paper, we use full-waveform 3-D synthetic data to consider the effects that 3-D topography on a reflector has on reflection character on a 2-D profile. We base our synthetics on an observed shear zone and test models with both a single layer and anastomizing layers. We show that topography on the reflector out of the plane of the section may cause spurious events both above and below the expected target depth. We derive the basic understanding using a simple isotropic homogeneous model, however, we then demonstrate that this is a robust phenomenon and is endemic on all 2-D sections even if the overburden is not homogeneous. We demonstrate that we obtain similar results with a velocity gradient or, for a more extreme case, with a 2-km-deep basin filled with low-velocity sediment. For crustal scale seismic profiles, in particular, the effect is pervasive as neither stacking nor migration can discriminate against out-of-plane energy and the 2-D stack represents the 3-D seismic response of a broad swath centred on the profile. However, we conclude that using the modelled data it is possible to identify qualitatively where there is significant contamination from out-of-plane topography and show examples from a shear zone in the Archaean Yilgarn Block in Western Australia.

Key words: crustal structure, deep seismic reflection, reflection seismology, seismic modelling, seismic structure.

INTRODUCTION

This paper presents results from research into the effects of out-of-plane structure on images from single (2-D) seismic profiles. Unlike contemporary oil industry practice, in which seismic data are now routinely collected as 3-D data sets and processed and migrated to produce accurate depth images of the subsurface, seismic reflection images of the deep crust are usually collected along single profiles. The cost of collecting 3-D data sets across deep structures is prohibitive, particularly on land, and especially if the data are to have sufficient coverage to account for migration aperture. Wherever possible, the 2-D profiles are oriented in a dip direction so that the structures being imaged can be assumed to be continuous out of the plane of the seismic section. On occasions cross lines are recorded to monitor out-of-plane changes in reflector geometry, or parallel lines are recorded, but too few are recorded and they are spaced too far apart to allow migration of the seismic data out of the plane of the seismic sections. Invariably, therefore, the data are processed and interpreted assuming that the structures being imaged are 2-D, and any effects of out-of-plane energy are ignored when the data are interpreted.

The impedance contrasts that give rise to strong reflections from the deep continental crust have been attributed variously to shear zones, mafic underplated rocks and fluid-filled cracks (e.g. Matthews & Cheadle 1986; Klemperer *et al.* 1987; Warner 1990; Brown *et al.* 1996; Makovsky *et al.* 1999). None of these are likely

to be truly 2-D in shape. This research was stimulated by a study of why shear zones appear the way they do in seismic sections. Shear zones often appear in seismic sections as laterally continuous bands of discontinuous reflections. The bands can extend for several hundred milliseconds on seismic time sections. We compared synthetic seismograms with data from a subhorizontal detachment surface in the Archaean Yilgarn Block in Western Australia. The detachment represents a structure for which several simplifying assumptions can be made in the modelling, as discussed below, although we believe the results have universal application. This paper focuses on the geometry of the reflections. The effects on reflector amplitude are addressed elsewhere (Drummond *et al.* 2004). The models and synthetic data would be representative of both faults (e.g. one rock type juxtaposed against another with a different seismic impedance) and broader shear zones in which highly strained, altered and anisotropic rock would anastomose between and around blocks of protolith (Jones & Nur 1982, 1984; Law & Snyder 1997). However, the models would equally be representative of other types of geological features with similar types of geometry, for example, sills, fluid-filled cracks and the Moho if it occurs as crustal rocks above mantle rocks.

Similar studies of this type have been attempted in the past. Blundell & Raynaud (1986), Raynaud (1988) and Cao & Kennett (1989) generated synthetic seismograms for reflections from surfaces with regular topography in the form of cosine functions. Cao *et al.* (1991) introduced randomly irregular surfaces. Fountain *et al.* (1984) and Blundell (1990) studied synthetic models of shear zones in which they attempted to include lateral variations in the thickness of interleaved protolith and deformed rock. All of these studies demonstrated that surfaces with 2-D and 3-D topography can produce waveforms in seismic sections that appear more complicated that the geometries of the reflecting surfaces. In particular, the stacked data were dominated by diffracted energy. None of the synthetic seismograms from these studies were migrated, because, in general, the modelling algorithms did not generate accurate estimates of the reflection and diffraction amplitudes. Therefore, none of the studies produced synthetic seismic sections that could be compared directly with the input model. Nor did the studies allow the interpreter to discriminate between in-plane and out-of-plane energy. Nevertheless they contributed to an intuitive feel for the likely reflection signature of shear zones in stacked seismic sections. A study by Mufti (1990) used a 3-D finite difference algorithm to model out-of-plane reflectivity for a basin setting but the paper is largely concerned with the managing of the large computer resources required for this program. More recently, Novais & Santos (2005) were still addressing the computer resource problem with a 2.5-D finite difference modelling program, which by definition cannot model out-of-plane reflectivity.

In our study, we used the phase-screen method as implemented by Wild & Hudson (1998) and Wild *et al.* (2000) for calculating the synthetic seismograms. The phase-screen method generates synthetic seismograms in which the amplitudes of the arrivals are sufficiently accurate to allow migration of the reflection sections and, for the first time, allows computation of synthetic seismograms on a desktop workstation for large and complex 3-D models. We generated data for 3-D models but we migrated the data in 2-D to provide insight into how shear zones should appear in deep crustal profiles, how we might identify them, and whether we can discriminate the effects of internal structure in the shear zone from reflections from other sources. This paper follows previous work by Hobbs (2003), which used synthetic data generated by the phase-screen method to look at reflectivity associated with crust formation at an oceanic spreading centre.

We demonstrate that the effects of even small amounts of out-of-plane structure can significantly distort the geometry of reflections. As expected, the distortion cannot be removed through data processing, including 2-D migration. In deep seismic reflection imaging, using single 2-D profiles, we must therefore learn to recognize and account for the effects of out-of-plane reflector topography. We erect a set of tests that could be applied to stacked and migrated seismic data from 2-D seismic profiles that may provide insight into whether out-of-plane structure is affecting reflection geometry.

AN EXAMPLE OF SHEAR ZONES REFLECTIONS

Fig. 1 contains stacked and post-stack migrated seismic images of part of a regional detachment in the Eastern Goldfields Province of the Archaean Yilgarn Block in Western Australia. The sections have no vertical exaggeration. The detachment has been imaged in a number of regional 2-D seismic profiles and extends over 100 km in an east–west direction (Swager *et al.* 1997) and for a comparable distance north–south (Goleby *et al.* 2000). Its depth ranges from 3 to 8 km, but it probably formed below 10 km depth before regional uplift and erosion occurred that brought crystalline rocks to the surface. It separates regional shortening and strike slip faulting in the upper crust from similar effects at a different length scale in the middle to lower crust (Drummond *et al.* 2000).

Detachment topography can best be described as a series of subhorizontal segments at different depths joined by ramps. Fig. 1 shows one of the subhorizontal segments. Gravity modelling using the geometries of rock bodies constrained by seismic reflection data and detailed structural mapping suggests that rocks of similar density lie above and below the detachment in this region (Swager *et al.* 1997). Also, the seismic reflection data do not require different seismic velocities above and below the detachment in this region. Therefore, the reflectivity of the detachment in this region is likely to arise from the intrinsic reflectivity of the detachment, and not from the juxtaposition of rocks of different seismic impedances on either side of the detachment. The detachment is, effectively, a subhorizontal shear zone. However, the detachment does have some limited local topographic relief, requiring us to study how small scale topography on the reflector can affect the seismic images of the shear zone. Because it is subhorizontal in this area, we can ignore the regional dip on the reflector and the effects this might have on the positions of the shear zone in stacked and migrated images when considering synthetic examples.

The top of the reflections from the detachment lies near 2.5 s two-way traveltime (TWT) in Fig. 1(a) and the reflections extend in TWT for 300–400 ms. The dashed hyperbolas plotted near the labels $\mathbf{P}'_1$ and $\mathbf{P}'_3$ are calculated diffraction curves for the plane of the section. They highlight diffractions that extend from the bottom of the band of energy reflected from the detachment. The crust below the detachment in this region is mostly non-reflective except for isolated diffractions, such as $\mathbf{P}'_2$ and $\mathbf{P}'_4$, for which the theoretical diffraction curves for this section are plotted as dashed lines. $\mathbf{R}_1$ is a reflection from a structure below the detachment. $\mathbf{R}_2$ is the reflection from a ramp in the detachment, which lies at a shallower level to the right of this figure. Apart from an allowance for geometric spreading of the wave front, the amplitudes of the seismic traces have had no time-varying amplitude scaling applied. The amplitudes

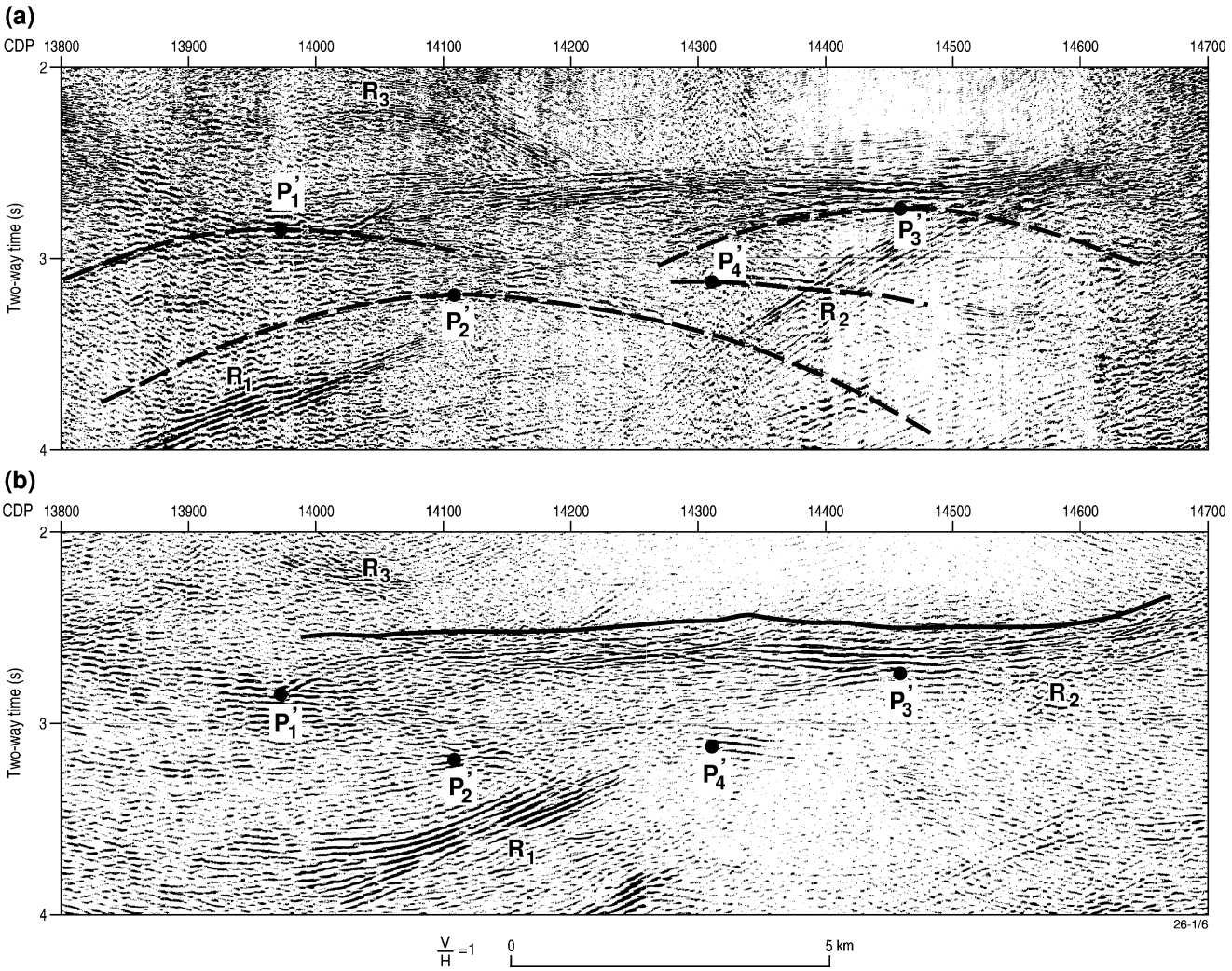

Figure 1. Example of a subhorizontal shear zone: part of a regional detachment surfce in the Eastern Goldfields Province of Western Australia (a) stacked, (b) 2-D post stack migrated. $\mathbf{P}'_1$ to $\mathbf{P}'_4$ label diffracted energy discussed in the text. Dashed lines in (a) indicate the predicted shape of diffractions; dots mark the top of the diffraction curve and are repeated in (b) to show where diffracted energy migrates. Solid line in (b) is the interpreted top of the reflections from the detachment. R1–R3 are label reflections.

and reflection character of the detachment surface in Fig. 1 are representative of the signature of the detachment surface regionally, and, we believe, of many other shear zones. That is, shear zones generally appear as semi-continuous bands of strong reflections in which individual reflections are not continuous across the full lateral extent of the band.

The preservation of pseudo-true amplitudes in Fig. 1(a) allowed the data to be post-stack migrated at stacking velocities to produce Fig. 1(b). The overall signature of the detachment has been preserved in the migrated section; that is, it still appears as a continuous band of discontinuous reflections with a TWT thickness of 300–400 ms. The top of the envelope of reflections from the detachment has of the order of 100 ms (TWT) topography, as in the stacked section, although the topography is greater where the ramp upwards begins at $\mathbf{R}_2$ at the right-hand side of the figure. Note that all diffracted energy has collapsed to small zones, or effectively points. $\mathbf{P}'_1$ and especially $\mathbf{P}'_3$ lie within the envelope of reflections from the detachment, with no energy extending downwards from the envelope of detachment reflections. Note also that $\mathbf{P}'_2$ and $\mathbf{P}'_4$ lie up to 500 ms below the top of the band of reflections from the detachment, and around 200 ms below the bottom of the band. $\mathbf{R}_1$ has steepened and moved up dip, as expected.

THE BEHAVIOUR OF OUT-OF-PLANE ENERGY—GEOMETRICAL CONSIDERATIONS

Traveltimes for an out-of-plane point reflector

In later sections, we use synthetic examples to illustrate the effects of reflector topography on the signature of reflections from shear zones. In order to understand the synthetic examples, it is useful to consider first the effects of a single point reflector.

Assume that **P** is a point reflector (diffractor) outside the plane of a 2-D seismic section (Fig. 2a). **P** lies in a medium with a homogeneous and isotropic velocity v. The TWT of reflections from **P** is, therefore, a linear function of the distance of the observation point from **P**.

In Fig. 2(a), the plane of the seismic section is through the origin and lies along the X axis. **P** lies at the coordinates $(0, y_1, t_1)$; that

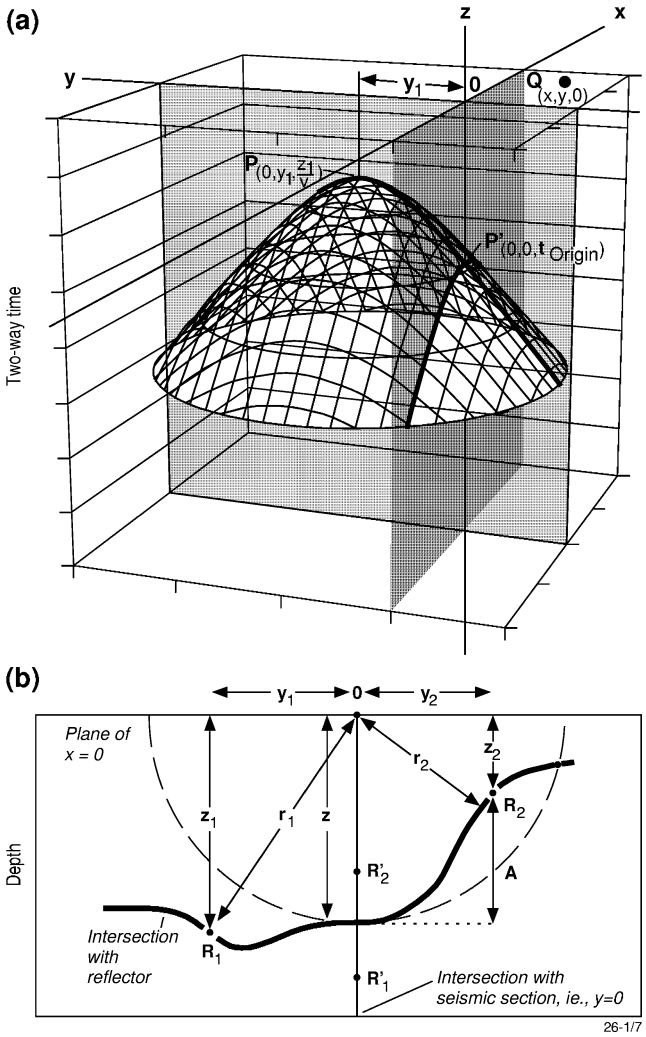

Figure 2. (a) Hyperbolic surface representing the shape of the diffraction from a point P lying out of the plane of the seismic section. (b) Cross-section normal to the plane of the seismic section showing the scenarios in which reflected energy from out of the plane of the section will be recorded before or after the reflection from in the plane. Dashed semicircle shows intersection of the plane of the diagram with a hemisphere centred on O and passing through the intersection of the reflector with the plane of the seismic section.

is, it lies on the Y axis at time $t_1 = z_1/v$ and at a distance y_1 from the origin. The traveltime t from any point **Q**(x,y,0) on the Earth's surface to **P** is defined by the equation

$$t = \frac{QP}{v} = \frac{\sqrt{x^2 + (y - y_1)^2 + z_1^2}}{v}, \tag{1}$$

where QP is the distance from the observation point **Q** to the point **P**.

This is a hyperbolic surface, as shown in Fig. 2(a). To migrate accurately the energy reflected from point **P**, all energy along this surface should be migrated in 3-D. However, in 2-D seismic imaging, only the energy in the plane of the section is migrated, based on the assumption that all energy in the section results from reflectors in the plane of the section.

At the origin ($x = y = z = 0$), the hyperbolic surface will be at a depth OP' such that

$$t_{\text{Origin}} = \frac{OP'}{v} = \frac{\sqrt{y_1^2 + z_1^2}}{v}. \tag{2}$$

The hyperbolic surface intersects the plane of the section at $y = 0$, so that from eq. (1), it cuts the plane of the section along a 2-D hyperbola of the form

$$t_{y=0} = \frac{\sqrt{x^2 + y_1^2 + z_1^2}}{v} = \frac{\sqrt{x^2 + OP'^2}}{v}. \tag{3}$$

This is also the equation for a diffraction in the plane of the section from point **P**′. Therefore, in the plane of the seismic section, the diffraction from point **P** produces a hyperbolic event which will perfectly migrate in 2-D with the correct velocity, v, to a point at **P**′, but point **P**′ is not the true origin of the diffraction and is at a spurious depth determined by the distance of the 2-D section from the original diffraction point **P**.

Implications for a point reflector

When using 2-D imaging and 2-D migration, we expect that energy from within the plane of the section will migrate to its correct position. However, eq. (3) demonstrates that energy from outside the plane of the section will also appear to migrate correctly. That is, reflected energy from out of the plane of the section migrates within the plane of the section, but the TWT and, therefore, the apparent depth of the reflector is different from its true depth out of the plane of the section. In this case it is deeper.

In Fig. 1, the diffracted energy labelled $\mathbf{P}'_1$ to $\mathbf{P}'_4$ might be examples of energy reflected from the detachment out of the plane of the seismic section that plots below the position of the detachment in the plane of the section. The tops of the diffraction hyperbola for $\mathbf{P}'_1$ and $\mathbf{P}'_3$ lie just below the top of the envelope of energy from the detachment, and the diffractors, therefore, would be close to the plane of the section. The top of $\mathbf{P}'_2$, however, lays approximately 0.5 s (TWT) below the top of the envelope. If it is an out-of-plane reflection from topography on the detachment interface, then it would originate from a portion of the detachment lying approximately 5.2 km out of the plane of the section.

Behaviour of a reflector with out-of-plane topography

A 3-D subhorizontal reflector with topography can be considered in terms of the behaviour of a series of point diffractors on the reflector. The time at which energy from out of the plane of the section will plot within the section is examined using Fig. 2(b), which shows diagrammatically the intersection of the plane of the seismic section ($x = 0$ km) with a subhorizontal reflector. Fig. 2(b) is a cross-section orthogonal to the plane of the seismic section. In general terms for an isotropic homogeneous subsurface, out-of-plane reflections will fall below the in-plane reflection if $r > z$ (as is the case for point R_1), at the same time as the in-plane reflection if $r = z$ (and reinforce the amplitude of the in-plane reflection), and above the in-plane reflection if $r < z$ (as is the case for point R_2). In the plane of Fig. 2(b), the equation $r = z$ represents a semicircle centred on the observation point **O**, with a radius equal to the depth of the reflector in the plane of the section z. In 3-D, it represents a hemispherical surface. In general, we expect energy from out-of-plane reflections will fall below the in-plane energy, that is, the reflection point lies outside the hemisphere. However, situations will exist where the reflector has sufficient out-of-plane relief, A, that parts of it lie within the hemisphere as defined by

$$A > z - \sqrt{z^2 - y^2}, \tag{4}$$

then the out-of-plane reflected energy from those parts will arrive before the in-plane energy.

Behaviour for non-homogeneous earth models

The analysis can be extended to encompass more general situations where there is a velocity gradient in the subsurface or low-velocity sedimentary layer at the surface. The imaging of out-of-plane energy is a function of the mean velocity between the profile and the out-of-plane diffraction point, the stacking and migration velocities in the 2-D section at the traveltime where the diffracted energy intersects with the section, and the distance of the diffractor from the profile. Stacking velocity becomes poorly constrained when the target depth exceeds the survey aperture, that is, there is not enough of the hyperbolic move-out curve recorded, and also temporal resolution is reduced because of preferential loss of high-frequency content due to effective Q. This statement can be recast as: stacking cannot discriminate between two events at the same TWT if the difference in stacking velocity is such that, at the maximum offset included in the stack, the difference in the NMO curve is less than half the minimum period of the source wavelet. By analogy a similar rule can be constructed for the migration operator, which means a migration operator will focus energy for two different diffractions provided the migration velocity difference is such that, at the maximum migration aperture, the time difference is less than half the minimum period of the source wavelet; here the aperture is affected by both acquisition and processing parameters. For deep seismic imaging both these conditions are fulfilled and we would expect the deep 2-D image to represent the reflectivity from a swath centred on the profile. The relationship between the aperture $\boldsymbol{x}$ (either the half-width of the migration aperture or the stack aperture) and the rms velocity in the plane of the section, $\boldsymbol{v}_{1\mathrm{rms}}$, at the time where the out-of-plane diffracted energy intersects with the profile, $\boldsymbol{t}_0$ is given by

$$x^2 \approx \frac{t_0 T}{\left(\frac{1}{v_{2\mathrm{rms}}^2} - \frac{1}{v_{1\mathrm{rms}}^2}\right)}, \tag{5}$$

where $\boldsymbol{v}_{2\mathrm{rms}}$ is the rms velocity to the out-of-plane scatter, and $\boldsymbol{T}$ is the dominant period of the source. This assumes that velocity increases with depth. The swath half-width can then be determined either by numerical methods given an arbitrary velocity–depth curve or analytically for predefined functions (Al-Chalabi 1997). If, for the data shown in Fig. 1, we use a linear velocity depth relationship with a surface velocity of 6.3 km s^{-1} and a velocity gradient of 0.022 s^{-1}, an aperture of 10 km and a maximum frequency in the source wavelet of 60 Hz, then the swath half-width would be about 3 km at a depth of 8 km. This swath half-width will be reduced in cases when the aperture is increased, the traveltime is reduced, the source has higher frequency content or there is a higher velocity gradient. Changes in the opposite sense will increase the swath half-width.

SYNTHETIC EXAMPLES

From the above, the interpretation that energy at $\mathbf{P}'_1$ to $\mathbf{P}'_4$ in Fig. 1 could be reflected from out-of-plane segments of the detachment is possible. Nevertheless, apart from recording more field data, we have no means of confirming the interpretation. The behaviour of out-of-plane energy can be studied more robustly by considering systematically a set of synthetic seismograms for known models of differing levels of complexity.

A reflector surface of the type described in Appendix 1 and shown in Fig. 3 was created. The maximum peak to trough topography on the surface was scaled to 250 m, but along any profile through the surface the maximum range would typically be less. The model used was 12.7 km square. This surface has a dominant wavelength of 4.2 km in the X direction and 5.1 km in the Y direction; these are similar to the wavelengths of the topography on the detachment in Fig. 1. The surface also includes a range of shorter wavelengths with smaller amplitudes and random phase shifts, so that it has a roughness that generates reflections from out of the plane of the seismic section.

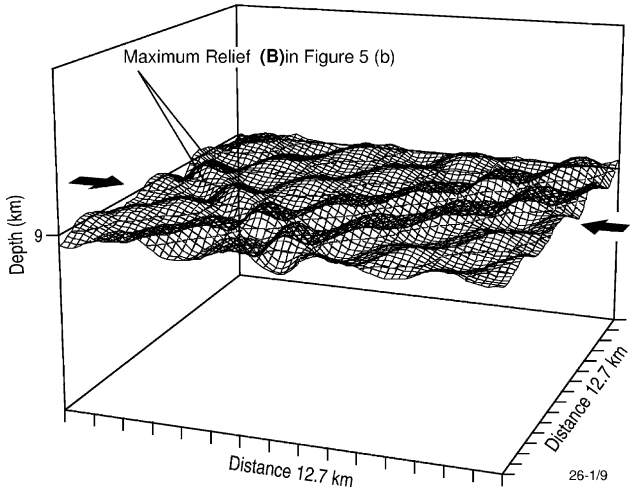

Figure 3. Surface of the form described in Appendix 1, from which a model of a shear zone layer was developed for subsequent synthetic seismogram modelling.

The surface was then used to construct a layer to represent a fault or thin shear zone by assigning a high seismic impedance (2000 kg m^{-2} s^{-1}) between two identical surfaces 50 m apart in depth. For the initial model, this layer was set in a homogeneous medium with a seismic velocity of 6.4 km s^{-1}. The layer was centred on 9 km depth, or around 2.8 s TWT, similar to the detachment in Fig. 1. Fig. 4(a) shows the layer in cross section. An identical thickness horizontal reference layer with equal impedance was placed at 7.92 km depth. With the data processed so that the amplitudes of the reference reflector were the same from the section from this model and sections from subsequent models discussed below, direct comparisons could be made between the amplitudes of reflections from a range of shear zone models. As shown in Fig. 4 and in later figures, the synthetic data have been plotted with a high gain to highlight diffracted energy. Therefore, the amplitudes of the reference reflection are clipped. The reader should use a comparison with the reference reflector with care; however, the clipping to reference amplitudes is only in the plotting process, and comparison of the shear zone reflector amplitudes between sections is valid.

In this study, two methods were used to calculate synthetic seismograms. In the first, a series of common shot gathers were calculated, sorted into CMP gathers and stacked. Secondly, synthetic seismograms were calculated along the same profile using an exploding reflector approach. This gave similar results to the CMP approach, and was computationally faster, so it was used for the calculation of all synthetic seismograms presented in this paper. The use of exploding reflector models (Loewenthal *et al.* 1976) is an accepted method to compute zero-offset data provided multiples are ignored as these will have the wrong traveltime (Claerbout 1985). Synthetic seismograms were calculated for a range of models in which the amount of structural complexity in the shear zone was systematically increased. All synthetic seismograms were migrated assuming the reflected energy came from within the plane of the

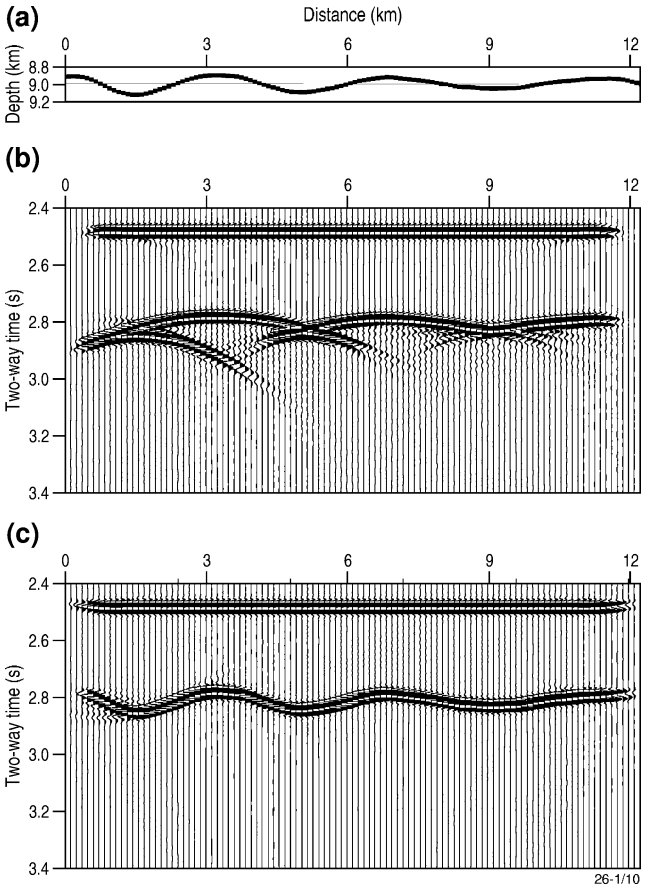

Figure 4. Seismic section from a 2-D shear zone layer at a depth comparable to the detachment in Fig. 1. (a) Cross-section at the scale of the seismic sections in (b) and (c). (b) Stacked and (c) 2-D migrated data.

section. That is, in order to simulate the conditions for regional 2-D seismic reflection surveys.

Two-dimensional reflector

Synthetic seismograms were calculated first for a 2-D model generated using the cross-section of the shear zone in the plane of the section. The model is shown in Fig. 4(a). The stacked section (Fig. 4b) shows concave downwards reflections across each antiform in the model, and characteristic strong diffractions below and to the sides of the synclinal parts of the shear zone. These diffractions have a form traditionally termed a 'bow tie', and each syncline generates one bow tie. When migrated (Fig. 4c), the synthetic data reproduced the shear zone geometry very well as a single reflection, apart from regions of numerical noise caused by the edge of the model and the resulting asymmetry in the diffractions at each end of the section. The migrated section in Fig. 4(c) provides a basis for comparison with sections from more structurally complex shear zone models.

Three-dimensional reflector

Synthetic seismograms were then calculated for a 3-D layer. The cross section in the plane of the seismic section for this model is the same as that in Fig. 4(a), but in and out of the plane of the section the shear zone layer has the topography shown in Fig. 3.

The geometry of the top of the reflections is dominated by antiforms and in the stacked data (Fig. 5a) appears similar to that for

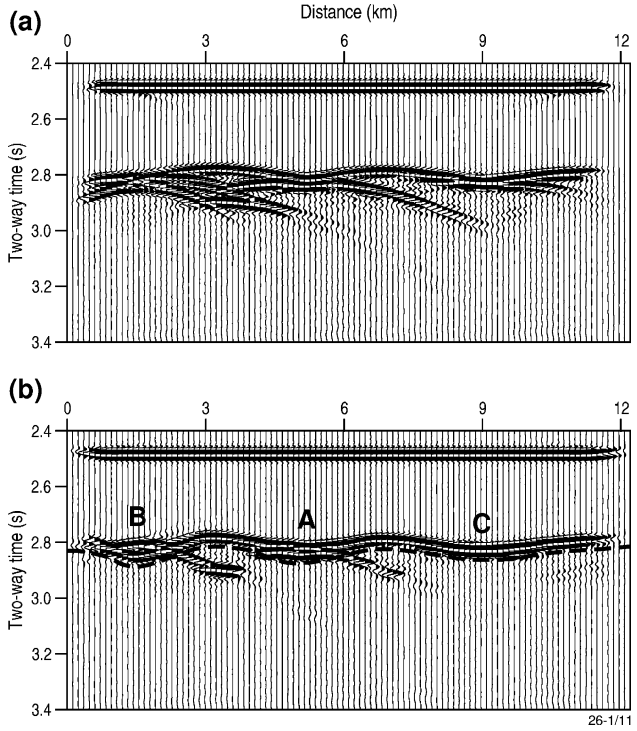

Figure 5. Seismic section from a 3-D shear zone layer. (a) Stacked and (b) 2-D Migrated data 'A', 'B' and 'C' in (b) are pointers to features discussed in the text.

the 2-D model in Fig. 4(b). However, the pattern of diffractions below the first reflections in Fig. 5(a) is not as simple. The bow ties that are present in Fig. 4(b) are also present in Fig. 5(a), but bow tie diffractions from synclinal keels outside the plane of the section are also present in the plane of the section. They inter-mingle and interfere with diffractions from the reflecting layer in the plane of the section. This is particularly clear under the synforms at the left and in the centre of the section.

The resultant differences in the migrated sections are quite marked. The dashed curve in Fig. 5(b) marks the bottom of the reflection in Fig. 4(c) from the 2-D reflector, and facilitates comparison of the two sections. In Fig. 4(c) no energy arrives below this level, in contrast with Fig. 5(b). The reflection from the 3-D shear zone layer is not a continuous first arrival reflection as in Fig. 4(c), although the dashed line allows identification of a reflection that marks the approximate position of the reflector. A first arrival reflection persists laterally across the centre and right of the seismic section, for example, below 'C' in Fig. 5(b). It comes from regions of the shear zone layer with topographic variations that are moderate and return out-of-plane energy that falls below the in-plane reflection. For the shear zone layer along the seismic section, the values in eq. 3 are $A \approx 0.22$ km, $y = 2.5$ km, and $z \approx 9.07$ km. The right-hand side of eq. (4) equates to 0.35 km, which is greater than A for this section. Therefore, along the bulk of the section, there is insufficient out-of-plane relief to cause reflections from out of the plane to plot above the expected position of the reflector in the plane of the section.

However, at the left-hand end of the section, just below 'B' in Fig. 5(b), some energy arrives before the continuous reflection that characterizes the geometry of the reflecting layer. This energy is identified because it lies above and is not coherent with the reflection that is continuous across the section. Near the left-hand end

of the section, interference between the various wavelengths that contribute to the topography of the layer leads to topographic relief out of the plane that is steeper than elsewhere. $A = 0.22$ km, $y = 1.18$ km, and $z \approx 9.07$ km. In this region, therefore, the right-hand side of eq. (4) gives a value of 0.08 km, which is less than A. Therefore, at the left-hand end of the section, out-of-plane relief is sufficient to cause out-of-plane reflections to fall above the expected position of the reflector in the section.

Finally, the reflection that is continuous across the section does not exactly reproduce the geometry of the reflector in the plane of the section. Just below 'A' in Fig. 5(b), the reflection is earlier than would be expected (the dashed line marks the position of the reflector in the plane of the section). This is because the seismic section lies diagonally across the side of a steep anticline. The sides of the anticlines form the part of the reflector normal to each recording point; the parts of the reflector immediately beneath the recording points are not horizontal and reflect energy out of the plane of the section.

Reflective zone rather than reflective layer—a 2-D case

Models of shear zones as broad zones in which bands of deformed rock wrap around and separate blocks of protolith can be built and modelled in 3-D. The model in Fig. 6(a) was generated using a layer defined by the same method as used for Figs 4 and 5, repeated eight times with random shifts in X, Y and Z. The maximum peak to trough topography of the layers was scaled variously between 62.5 and 250 m across the whole model, and the thickness of the layers was varied between 10 and 50 m. In three of the layers the topography was inverted. This produced a zone of reflectors which had no correlation in structure from layer to layer. The layers represented mylonitic rocks, and the regions between the layers represented protolith. The zone of reflectors represented by Fig. 6(a) is around 250 m thick. Real mylonite zones might consist of several such bands that range in thickness from a few metres to hundreds of metres across, separated by protolith, and with a total width reaching several kilometres (e.g. see the models of Fountain *et al.* 1984 and Blundell 1990).

Synthetic seismograms were calculated first for a 2-D slice through this model in the same way as Fig. 4. The cross-section is shown in Fig. 6(a) with the stacked data in Fig. 6(b) and the 2-D migrated data in Fig. 6(c). Reflections from a reference reflector lie at the tops of the figures.

A marked difference between the stacked data for this model and those for a single layer is the number of diffractions, or bow ties. Whereas Fig. 4(b) has bow-tie diffractions from the bottoms of each of 3 synforms, Fig. 6(b) has many bow-tie diffractions because the synforms in each layer generate diffractions. Several have much higher amplitudes than others, and in places they destructively interfere. The data migrate to form a band with a clear top and bottom defined by the reflectors that bound the band (Fig. 6c), but the internal geometry of the reflectors is not discernible in the data at the frequencies and wavelengths used in this modelling.

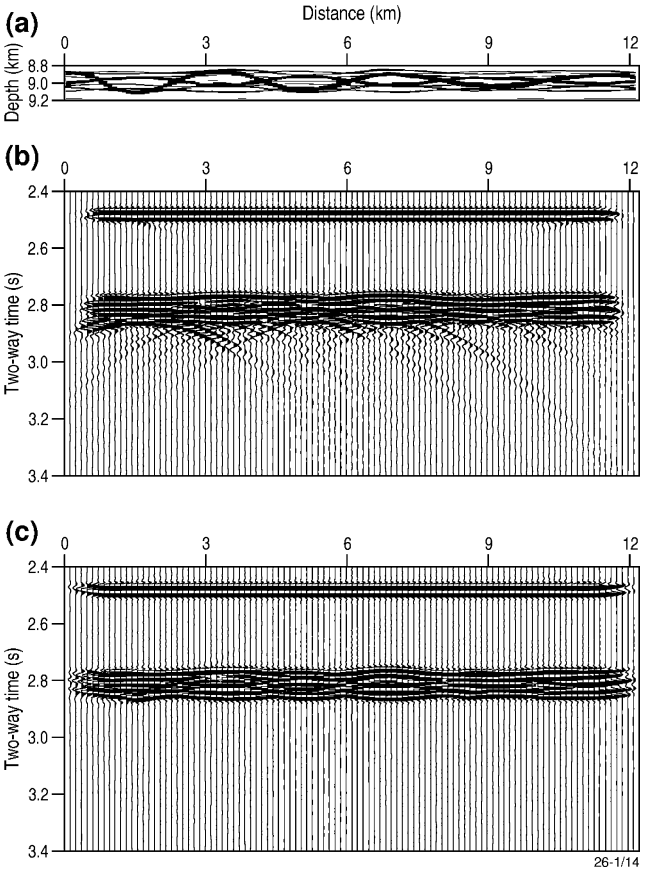

Figure 6. Reflections from multiple layers in a 2-D shear zone (a) cross-section of the shear zone, (b) stacked data and (c) 2-D migrated data.

Reflective zone rather than reflective layer—a 3-D case

The synthetics were then recomputed using the full 3-D model. Stacked data are shown in Fig. 7(a), and migrated data are shown in Fig. 7(b). The reference reflection is at the top of each section.

The stacked data (Fig. 7a) have weaker diffractions compared to Figs 4(b), 5(a) and 6(b). This is because many diffractions from point reflectors come into the plane of the section, and because the

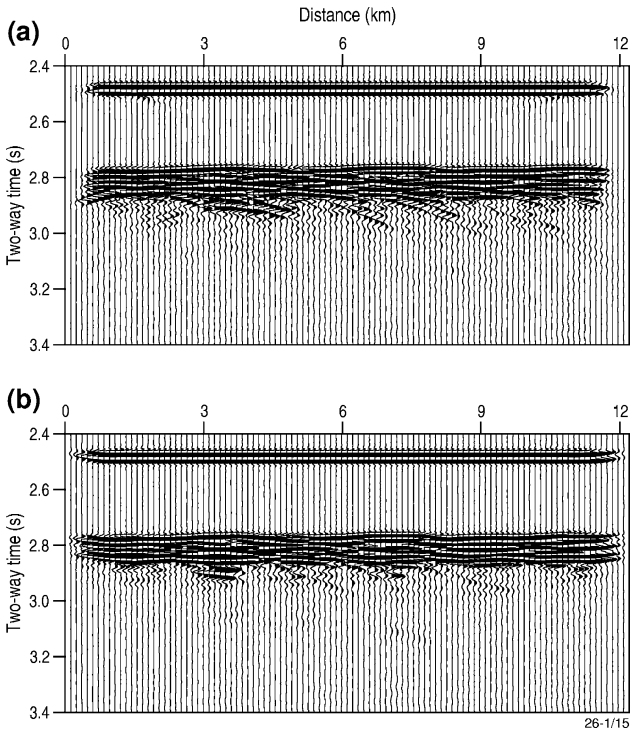

Figure 7. Reflections from multiple layers in a 3-D shear zone (a) stacked data (b) 2-D migrated data.

variations in arrival times mostly destructively interfere or cause the diffractions to have an apparent lower frequency content. When the data are migrated (Fig. 7b), the lack of diffracted energy results in poor resolution of the bottom of the reflective band, so that, instead of being a sharp boundary as in Fig. 6(c), it is more diffuse.

Three-dimensional reflector with non-homogenous background velocity modelling

To test the sensitivity of the effect with non-homogeneous background models, two tests were carried out. The first model uses a simple velocity gradient starting at 6.3 km s^{-1} at the surface with a gradient of 0.0222 s^{-1}, which gives an interval velocity of 6.5 km s^{-1} at the target depth of 9 km and a migration velocity of 6.4 km s^{-1} at the target time of 2.8 s; the second model introduces a 2 km thick basin filled with 2 km s^{-1} sediments at the surface, the target reflector is kept at 9 km with a basement velocity of 6.4 km s^{-1}, here the migration velocity is 4.83 km s^{-1} at the target time of 4.2 s. In both cases the impedance of the target is the same as for the previous models. The 2-D images of the 3-D surface for both models are shown in Figs 8(b) and (c), respectively. Comparisons with the equivalent homogeneous model (Fig. 8a), shows that the imaging issues are robust despite the variation in overburden velocity model.

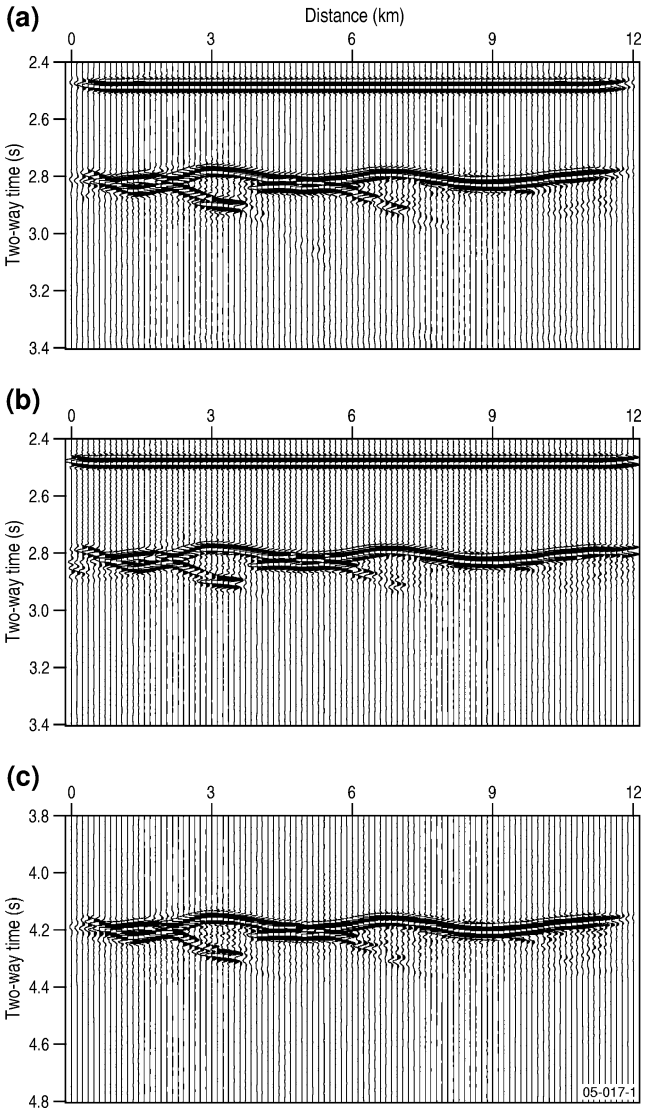

Figure 8. Comparison of the 2-D image of a 3-D single reflector with different background velocities: (a) a homogeneous velocity of 6.4 km s^{-1}, (b) a velocity gradient with a surface velocity of 6.3 km s^{-1} and a gradient of 0.0222 s^{-1} and (c) a 2 layer velocity with a 2-km-thick 'basin' with a velocity of 2.0 km s^{-1} over basement with a velocity of 6.4 km s^{-1}. Target layer is at 9 km depth for all cases.

DISCUSSION

The initial analysis of the effects of 3-D structure in 2-D seismic profiles presented in this paper is based on the assumption that the Earth can be approximated by an isotropic homogeneous half space above reflectors, as it simplifies both the derivation of eq. (4) and the visualization of the region from which reflector topography will cause out-of-plane reflections. Other velocity functions would change the values of out-of-plane offset and topographic relief that would cause the out-of-plane reflection to be recorded before or after the in-plane reflection, however, the principles established for the simple model are still relevant; that is, out-of-plane energy will behave as if it came from within the plane of the section provided eq. (5) is fulfilled. A qualitative interpretation of the reflections is Figs 4, 5, 6, 7 and 8 is, therefore, relevant no matter what velocity function is used. The interpretation is summarized in Table 1.

In 2-D, single-layer reflectors produce relatively simple diffraction or 'bow-tie' patterns in the stacked sections, with a bow tie for each synform. When 3-D structure is introduced, the number of diffractions or bow ties increases because bow ties are also recorded for the synforms out of the plane of the section. The times at which the out-of-plane bow ties are recorded for a homogeneous model are defined by eq. (4). The migrated data for single-layer reflectors are characterized by relatively continuous reflections. For 2-D reflectors, that is, no out-of-plane topography, the reflection response is a single reflection at the predicted time of the reflector in the plane of the section. When 3-D structure is present (Fig. 5), the reflection character is still dominated by laterally continuous reflections, but their positions in the seismic section are not accurate predictors of the position of the reflector in the plane of the section. Changing the background velocity from a homogeneous to a more complex structure makes little difference to the migrated image as shown in Fig. 8. eq. (5) predicts the permissible velocity perturbation which can then be used to estimate the swath width that may contain out-of-plane reflections that will migrate as if they where in the plane of the section. Calculation of this swath-width is complex and is dependent on the details of the velocity model on a case by case basis. However, eq. (5) implies that for deep seismic imaging or other targets where there are only weak velocity variations the swath-width will be large with little discrimination of out-of-plane energy.

Multiple-layer reflection zones produce many more diffractions, or bow ties, than single layer reflectors because a diffraction is created for every synform for every layer. They destructively interfere at depths below the expected depth of the reflector in the plane of the section (Figs 6b and 7a), and diffractions appear to have lower amplitudes than those for single layers (Figs 4b and 5a). These effects are more marked for 3-D zones (Fig. 7a) than for 2-D reflection zones (Fig. 6b). When migrated, the top of the band of reflections can be distinct (Figs 6c and 7b). For 2-D models it predicts the position of the top of the reflector zone in the plane of the section, but becomes increasingly unreliable as a predictor as the amount of topographic relief increases. The bottom of the reflection zone is distinct for 2-D zones (Fig. 6c), but less so for 3-D zones (Fig. 7b).

Table 1. Summary of the difference between single layer and reflective zones, and between 2-D and 3-D models imaged and processed in 2-D.

Differences—single layer & zone of many layers	
Single layer	Zone of many layers
Relatively long, sinuous reflections	Many short reflections
Differences — 2-D and 3-D	
2-D model	3-D model
Single layer in 2-D produces single reflection at the correct TWT	Single layer in 3-D produces band containing many sinuous reflections; • Seismic image is poor predictor of reflector position • Increasing the 3-D topography increases the thickness of the band of reflections
Bow tie for each synform crossed by the seismic section, therefore, few bow ties • Amplitudes of bow ties are high	Bow ties for synforms both in and out of the plane of the section, therefore, many more diffractions than synforms apparent in the structure of the reflector; • diffractions tend to destructively intefere and are relatively weak
Multiple layers produce thick reflection band with a clear bottom	Multiple layers produce no sharply defined bottom to reflection band

These results allow us to build a set of qualitative tests for 2-D and 3-D topography, and for single and multiple layered shear zones. The first discriminator that could be applied is the length of individual reflections: in migrated data, single reflectors will produce reflections that are laterally more continuous than multiple layer shear zones. An increase in the thickness of the band of more continuous reflections provides an indication of an increasing amount of out-of-plane topographic relief on a single reflector. A thick band of reflections indicates more relief (in terms of amplitude and number of synforms and antiforms) than a thin band of reflections.

If the reflections form a band in which individual reflections are laterally short, then the reflections are more likely to come from a zone of reflectors rather than a single reflector. In the Earth, such features are more likely to be 3-D than 2-D, but as a test a 3-D zone would have a poorly resolved lower boundary compared to a 2-D zone.

Having used migrated data to discriminate between single layers and multiple layers, and 2-D and 3-D topographic relief, the stacked data can be used provide some additional tests. A single 2-D layer will produce a bow tie for each synform evident in the migrated section. If the single layer had 3-D relief, there will more bow-tie diffractions than observed synforms and some individual bow-tie amplitudes will be high. If the reflections come from a zone of reflectors rather than a single reflector, there will be numerous diffractions, but the typical bow-tie form will be less obvious, and the strength of the diffractions will be weak, particularly for 3-D multiple layer zones, because of the destructive interference caused by so many diffractions.

This summary allows us to examine the reflection character of the regional detachment imaged in the Eastern Goldfields Province of Western Australia shown in Fig. 1, and to interpret the likely nature of the reflector. Fig. 9 shows distinctly different examples of the reflection character of data from two parts of the detachment from one regional deep seismic profile. In Fig. 9(a), stacked data show part of the detachment. Note that the detachment is faulted between F and F′. Diffraction D is from a diffractor off the end of the section and, therefore, does not migrate properly because the section does not contain all of the diffracted energy. In the migrated data (Fig. 9b), the reflections that define the detachment are long and continuous. The band of reflections is thin (only about 200 ms thick). The top of the band of reflections is distinct. The bottom is less distinct, but reflections at the bottom appear to be discrete and fully migrated. The reflected energy from the detachment has only a few, strong diffractions. This part of the detachment has the characteristics of a single reflector with some 3-D out-of-plane topography that cause a thin band of reflections within the plane of the section.

The reflection character of the detachment shown in Figs 9(c) (stacked data) and (d) (migrated) is distinctly different from that in Figs 9(a) and (b). The stacked data have numerous diffractions, mostly dipping to the right. The band of reflections from the detachment is thicker than in Figs 9(a) and (b), and individual reflections tend to have less lateral continuity. The top and bottom of the band of reflections in the migrated data are more diffuse than in Fig. 9(b); the bottom has the appearance of being slightly undermigrated. The detachment dips to the left in this region, and left-dipping diffractions may be coincident with non-diffracted energy. In this region, the reflection character of the detachment is more consistent with a broad zone consisting of a number of reflectors with topography in and out of the plane of the section, rather than a single reflector.

The common practice in acquiring, processing and interpreting regional deep seismic lines is to acknowledge that the Earth is 3-D, but in imaging the Earth using 2-D techniques we have until now not had the mechanism to understand fully the effect of the 3-D structure in our 2-D sections. In this work, we have been able to describe the effects of energy coming into the plane of the section. We have considered the effects on the shape of the reflections from single reflectors and from shear zones made up of multiple reflectors. This work and the examples of reflection character of the detachment from the Eastern Goldfields Province of Western Australia suggest that it should be possible to distinguish between 2-D and 3-D shear zones, and between shear zones that are single layers and those that have multiple layers. The results have implications for other kinds

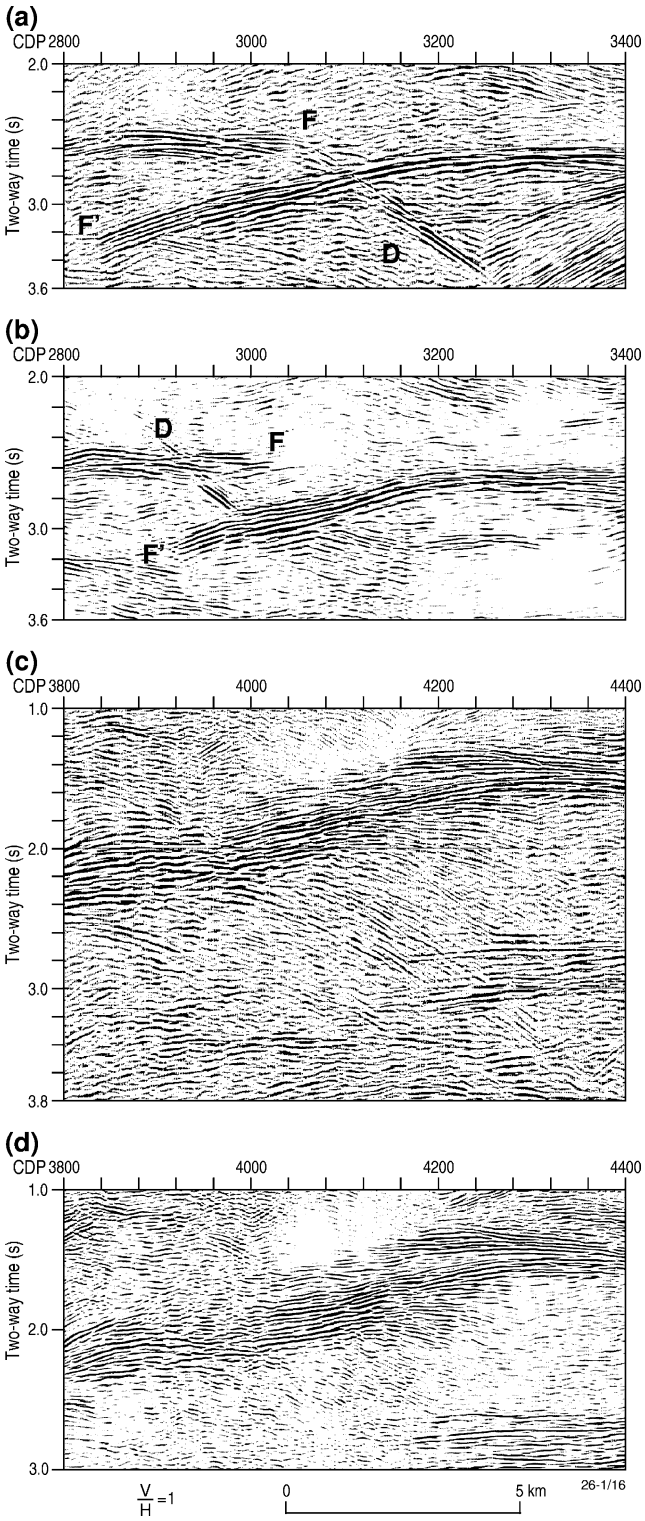

Figure 9. Two pairs of stacked and post stack 2-D migrated portions of a seismic image of the detachment in the Eastern Goldfields Province to the north of the position of the data shown in Fig. 1(a) and (b) show limited numbers of diffractions and a migrated signature with a few reflections that are laterally continuous. Most likely a single reflector or layer with limited 3-D topography. (c) and (d) have many diffractions, and a migrated signature with many reflections that are laterally less continuous than in (b). The top and particularly the bottom of the zone of reflections are less distinct in (d) than in (b). Possible a shear zone with multiple internal reflectors.

of reflectors. For example, the Moho and sheet intrusions would be examples of structures that are often imaged as continuous bands of discontinuous reflections, which may come from a single interface or multiple layers with only moderate topography in and out of the plane of the section.

ACKNOWLEDGMENTS

The seismic sections were plotted using Seismic Unix software available from the Colorado School of Mines. Joe Mifsud and Angie Jaensch prepared the diagrams. BJD and BRG publish with the permission of the Chief Executive Officer of Geoscience Australia. Neil Goulty for mathematical support; and reviewers, Richard England in particular, for their constructive comment.

REFERENCES

Al-Chalabi, M., 1997. Time-depth relationships for multilayer depth conversion. *Geophys. Prospect.,* **45**(4), 715–720.

Blundell, D.J., 1990. Seismic images of continental lithosphere. *J geol Soc. Lond.,* **147,** 895–913.

Blundell, D.J. & Raynaud, B., 1986. Modelling lower crust reflections observed on BIRPS profiles. In Reflection Seismology: a global perspective, ed. Barazangi, M., American Geophysical Union, Geodynamics Series, **13,** 287–295.

Brown, L.D. *et al.*, 1996. Bright spots, structure, and magmatism in Southern Tibet from INDEPTH Seismic Reflection Profiling. *Science,* 274.

Cao, S. & Kennett, B.L.N., 1989. Reflection seismograms in a 3-D elastic model: an isochronal approach. *Geophys. J. Int.,* **99,** 63–80.

Cao, S., Goleby, B.R. & Kennett, B.L.N., 1991. Modelling seismic reflections in central Australia by the 3-D isochronal technique. *Exploration Geophysics,* **22,** 525–532.

Claerbout, J.F., 1985. Imaging the Earth's Interior. *Blackwell Scientific Publ*.

Drummond, B.J., Goleby, B.R. & Swager, C.P., 2000. Crustal signature of Late Archaean tectonic episodes in the Yilgarn craton, Western Australia: evidence from deep seismic sounding. *Tectonophysics,* **329,** 193–221.

Drummond, B.J., Hobbs, R.W. & Goleby, B.R., 2004. The effects of out-of-plane seismic energy on reflections in crustal-scale 2-D seismic sections. *Tectonophysics,* **388,** 213–244.

Fountain, D.M., Hurich, C.A. & Smithson, S.B., 1984. Seismic reflectivity of mylonite zones in the crust. *Geology,* **12,** 195–198.

Goleby, B.R. *et al.*, 2000. Crustal structure and fluid flow in the Eastern Goldfields, Western Australia. Australian Geological Survey Organisation, Record, 2000/34.

Hobbs, R., Tong, C.H. & Pye, J., 2003. Modelling and processing of 3-D seismic data collected over the Overlapping Spreading Centre on the East Pacific Rise at 9 03′N, *New Insights into Structural Interpretation and Modelling,* Special Publication of The Geological Society, London, **212,** 251–259.

Jones, T.D. & Nur, A., 1982. Seismic velocity and anisotropy in mylonites and the reflectivity of deep crustal fault zones. *Geology,* **10,** 260–263.

Jones, T.D. & Nur, A., 1984. The nature of seismic reflections from deep crustal fault zones. *J. geophys. Res.,* **89,** 3153–3171.

Klemperer, S.L. & the BIRPS Group, 1987. Reflectivity of the crystalline crust: hypotheses and tests. *Geophys. J. R. astr. Soc.,* **89,** 217–222.

Law, A. & Snyder, D.B., 1997. Reflections from a mylonitized zone in central Sweden. *J. geophys. Res.,* **102,** 8411–8425.

Loewenthal, D., Lu, L., Roberson, R. & Sherwood, J., 1976. The wave equation applied to migration: *Geophys. Prospect.,* **24,** 380–399.

Makovsky, Y. & Klemperer, S.L., 1999. Measuring the seismic properties of Tibetan bright spots: evidence for free aqueous fluids in the Tibetan middle crust. *J. geophys. Res.,* **104**(B5), 10 795–10 825.

Matthews, D.H. & Cheadle, M.J., 1986. Deep reflections from the Caledonides and Variscides west of Britain and comparison with the Himalayas, in eds Barazangi, M. & Brown, L., *Reflection Seismology: A*

Global Perspective. American Geophysical Union, Geodynamics Series, **13,** 5–19.

Mufti, I.R., 1990. Large-scale three-dimensional seismic models and their interpretive significance: *Geophys. Soc. of Expl. Geophys.,* **55,** 1166–1182.

Novais, A.N. & Santos, L.T., 2005. 2.5D finite-difference solution of the acoustic wave equation. *Geophys. Prospect.*, **53**(4), 523–531. 10.1111/j.1365-2478.2005.00488.x

Raynaud, B., 1988. Diffraction modelling of 3-D lower-crust reflectors. *Geophysical Journal,* **93,** 149–161.

Swager, C.P., Goleby, B.R., Drummond, B.J., Rattenbury, M.S. & Williams, P.R., 1997. Crustal structure of granite-greenstone terranes in the Eastern Goldfields, Yilgarn Craton, as revealed by seismic reflection profiling. *Precambrian Research,* **83**(1–3), 43–56.

Warner, M., 1990. Basalts, water or shear zones in the lower continental crust? *Tectonophysics* **173,** 163–174.

Wild, A.J. & Hudson, J.A., 1998. A geometrical approach to the elastic complex screen. *J. geophys. Res.,* **103,** 707–725.

Wild, A.J., Hobbs, R.W. & Frenje, L., 2000. Modelling complex media: an introduction to the phase-screen method. Physics of the Earth and Planetary Interiors, **120,** 219–225.

APPENDIX

A double Fourier surface can be written in the form

$$Z_{x,y} = \sum_{i=1}^{n} \begin{pmatrix} a_i \sin(\frac{2\pi x}{\lambda_{xi}} + \theta_{xi}).b_i \sin(\frac{2\pi y}{\lambda_{yi}} + \theta_{yi}) + a_i \sin(\frac{2\pi x}{\lambda_{xi}} + \theta_{xi}).b_i \cos(\frac{2\pi y}{\lambda_{yi}} + \theta_{yi}) + \\ a_i \cos(\frac{2\pi x}{\lambda_{xi}} + \theta_{xi}).b_i \sin(\frac{2\pi y}{\lambda_{yi}} + \theta_{yi}) + a_i \cos(\frac{2\pi x}{\lambda_{xi}} + \theta_{xi}).b_i \cos(\frac{2\pi y}{\lambda_{yi}} + \theta_{yi}) \end{pmatrix} \quad \text{(A1.1)}$$

where

$Z_{x,y}$ = is the surface height at point x, y,
λ_{xi}, λ_{yi} = wavelengths in the x and y directions,
θ_{xi}, θ_{yi} = random phase shifts applied to each wavelength to make tuning unlikely and maximize roughness, and
a_i, b_i = amplitude attenuation factors of the form

$$a_i, b_i = e^{-\pi l} \quad \text{(A1.2)}$$

where

$$l = \frac{\lambda_n - \lambda_1}{\lambda_n - \lambda_i} \quad . \quad \text{(A1.3)}$$

This equation allows a surface to be built containing a range of wavelengths, with weighting given to each wavelength. The example in Fig. 3 has a range of wavelengths from 4200 m down to 420 m, in the X direction, and wavelengths 1.2 times this in the Y direction; that is, the longest wavelength was determined by the topography on the detachment in Fig. 1, and the shortest wavelength was less than the diameter of the first Fresnel zone for reasonable seismic frequencies at the depth of investigation. This produced a surface that was still semi-regular, but with a 'roughness' generated by the inclusion of shorter wavelengths with variable amplitudes and phase shifts. The higher wavelengths were attenuated according to equations A1.2 and A1.3 so that the amplitudes of shorter wavelengths did not dominate the surface roughness.